Microstructural and antibacterial properties of zinc-substituted cobalt ferrite nanopowders synthesized by sol-gel methods

Noppakun Sanpo,[1] Christopher C. Berndt,[1,2] and James Wang[1,a)]
[1]*Industrial Research Institute Swinburne, Faculty of Engineering and Industrial Sciences, Swinburne University of Technology, Hawthorn, VIC 3122, Australia*
[2]*Adjunct Professor, Stony Brook University, Materials Science and Engineering, Stony Brook, New York 11794, USA*

(Received 13 June 2012; accepted 3 October 2012; published online 26 October 2012)

Zinc-substituted cobalt ferrite nanopowders were prepared *via* a sol-gel route using citric acid as a chelating agent. The influence of zinc concentration on the microstructure, crystal structure, surface wettability, surface roughness, and antibacterial property of zinc-substituted cobalt ferrite nanopowders was investigated systematically. The substitution of zinc influences slightly the microstructure, surface wettability, surface roughness, and crystal structure but strongly affects the antibacterial property of the cobalt ferrite nanopowders. © *2012 American Institute of Physics*. [http://dx.doi.org/10.1063/1.4761987]

INTRODUCTION

Cobalt ferrite ($CoFe_2O_4$) exhibits a high coercivity of more than 5 kOe, a moderate saturation magnetisation of about 80 emu/g, excellent chemical stability and mechanical hardness, a large magneto-optic effect, a high Curie temperature, and high electromagnetic performance.[1,2] Therefore, cobalt ferrite is a promising candidate material for high density magnetic recording,[3] ferrofluids technology,[4] biomedical drug delivery,[5] magnetic resonance imaging,[6] data storage, biosensors,[7] biocompatible magnetic nanoparticles for cancer treatment,[8] and magneto-optical devices.[9] The substitution of Co^{2+} into cobalt ferrite with, for example, Zn^{2+}, Ni^{2+}, and Cu^{2+} allows variations in their properties that can be tuned to specific applications. Vaidyanathan and Sendhilnathan[10] demonstrated that when Co^{2+} was substituted with Zn^{2+} in $CoFe_2O_4$, the new $Co_xZn_{(1-x)}Fe_2O_4$ nanoparticles exhibited enhanced properties, e.g., excellent chemical stability, high corrosion resistivity, magneto-crystalline anisotropy, magnetostriction, and magneto-optical characteristics.

The special properties of magnetic nanoparticles required for biomedical applications demand precise control of particle size, shape, dispersion, and conditions that influence these properties. In principle, it is necessary to stabilize the magnetic nanoparticle dispersion in the aqueous environment. Thus, coating the magnetic nanoparticles with a polymer shell, including organic (polyethylene glycol, dextran, chitosan, polyethyleneimine, and phospholipids) or inorganic (silica) materials, is usually the first step that leads to highly dispersed and high quality nanoparticles with good biocompatibility.[11]

Buteică *et al.*[12] prepared the magnetic, core-shelled Fe_3O_4 nanoparticles to improve colloidal dispersion and to control particle sizes. Oleic acid was used as surfactant to coat the Fe_3O_4 nanoparticles, followed by an adsorption-coating with four different antibiotics (cephalosporins). The bacterial activity was tested on two different germs: *Escherichia coli* (*E. coli*) and *Staphilococcus aureus* (*S. aureus*). It was observed that, for the same time interval, the inhibition zone diameters for cephalosporins were higher than those for the cephalosporin-nanofluid. The nanofluid acted only as a carrier for the antibiotic.

In addition, small magnetic nanoparticles allow deliver of an antibiotic when targeting certain organs, such as the brain and kidney. Sun *et al.*[13] developed a thermal decomposition method that used a mixture of an iron salt, 1,2-hexadecanediol, oleic acid, oleylamine, and biphenyl ether to obtain Fe_3O_4 nanoparticles. The Fe_3O_4 nanoparticles were then coated with silver to improve bacterial activity. The paramagnetic properties of the nanostructures permitted recovery and recycling from the site of action by means of an external magnetic field.

Zinc-substituted cobalt ferrite nanopowders ($Co_{(1-x)}Zn_xFe_2O_4$ with $x = 0$, 0.3, 0.5, 0.7, and 1) were prepared by a variety of preparation techniques, including combustion,[14] chemical co-precipitation,[15] and microwave synthesis;[16] but the sol-gel method is considered the best way to produce homogeneous nanopowders.[17] Note that when $x = 0$ and 1, there is no atomic substitution; but we use terminology for convenience only. The sol-gel technique offers precise control over homogeneity, elemental composition, and powder morphology with uniformly distributed nano-sized metal clusters that are crucial for enhancing the properties of the nanopowders. These advantages make the sol-gel route a favourable alternative to other conventional methods for the preparation of ceramic oxide composites.[18]

Cobalt ferrite exhibits an inverse spinel structure with Co^{2+} in octahedral sites and Fe^{3+} equally distributed between tetrahedral and octahedral sites. The compound $ZnFe_2O_4$ demonstrates a normal spinel structure with Zn^{2+} in tetrahedral and Fe^{3+} in octahedral sites.[19] Therefore, zinc substitution in $CoFe_2O_4$ may have a distorted spinel structure that hinges on the concentration of the precursor solutions.

There have been few reports that investigate the effect of zinc concentration on the microstructure and magnetic properties of zinc-substituted cobalt ferrite nanopowders.[20] One study found that the magnetic properties of a spinel were

a)Electronic mail: JAWang@swin.edu.au.

sensitive to the types of cation and their distribution among the two interstitial sites of the spinel lattice.[21] Another claimed that the substitution of Zn^{2+} for Fe^{3+} reduced the Curie temperature of the ferrite.[22,23] However, no report has mentioned the use of these magnetic nanopowders for the biomedical field. Therefore, the objective of this study was to develop novel multifunctional magnetic iron-based nanopowders that also exhibit antibacterial properties to fulfil the requirements of a drug delivery system so that the antibiotic concentration could be minimized. For this purpose, we synthesized zinc-substituted cobalt ferrite nanopowders ($Co_{(1-x)}Zn_xFe_2O_4$ with $x = 0$, 0.3, 0.5, 0.7, and 1) by the sol-gel process using citric acid (CA) as a chelating agent. The effect of zinc substitution on surface morphology, size distribution, surface wettability, surface roughness, and antibacterial properties of the synthesized zinc-substituted cobalt ferrite nanopowders was systematically investigated.

METHODS AND PROCEDURES

Preparation of zinc-substituted cobalt ferrite nanopowders

The chelating agent, which is citric acid gel, was prepared by dissolving citric acid powders in distilled water (5%, w/v) at 70 °C. The chelating agent solutions were kept at 70 °C for 5 h or until the solution became clear. Cobalt nitrate ($Co(NO_3)_2\ 6H_2O$), iron nitrate ($Fe(NO_3)_3\ 9H_2O$), and zinc nitrate ($Zn(NO_3)_2\ 6H_2O$) powders with Fe:Co:Zn mole ratios of $2:(x):(1-x)$ (with $x = 0$, 0.3, 0.5, 0.7, and 1) were dissolved into the chelating agent solution under magnetic stirring. The sol-gel reaction was continued for 3 h and then the temperature increased to 80 °C for 10 h or until the gel dried into powder form. Finally, all samples were sintered at 800 °C for 4 h and then ground to form a nanopowder.

Characterization of samples

Elemental composition analyses of the zinc-substituted cobalt ferrite nanopowders were performed using energy dispersive x-ray spectroscopy (EDX). Raman spectroscopy examined the structure of the matrix in the composites. Phase analyses of the nanopowders were carried out using x-ray diffraction (XRD). Thermogravimetric analysis (TGA) and differential scanning calorimetry (DSC) were conducted in air to determine the temperature for the decomposition and oxidation of the chelating agent. Surface wettability was measured using the water contact angle technique (WCA-FTA200). The surface roughness of all nanopowders was measured using an AlphaStep-D-120 Stylus Profiler (KLA-Tencor Instruments). The morphology, i.e., homogeneity and particle size, of the nanopowders was observed using a field emission scanning electron microscope (FeSEM ZEISS SUPRA 40 VP).

The antimicrobial activity of zinc-substituted cobalt ferrite nanopowders was tested against gram negative bacteria, *E. coli*, and gram positive bacteria, *S. aureus*. The bacteriological test series were carried out according to the modified ASTM E2180-07; "Standard Test Method for Determining the Activity of Incorporated Antimicrobial Agent(s) in Polymeric or Hydrophilic Materials." All tests were performed on solid agar plates with the various zinc-substituted cobalt ferrite nanopowders. *E. coli* and *S. aureus* were grown aerobically at 37 °C overnight (OVN) with shaking (200 rpm) in an ordinary broth medium. The optical density (OD) of the overnight culture was measured at 600 nm by UV spectrometry and diluted with lysogeny broth (LB) to achieve an OD of 0.1. The diluted OVN culture was then seeded into the 20 ml LB (in a 50 ml falcon tube) and incubated at 37 °C on the shaker for 2 h to obtain an OD of 0.3. At OD = 0.3, the diluted OVN culture and cobalt ferrite nanopowders were further incubated for 24 h and 100 μl of the mixtures were spread on an agar plate using an L shaped spreader.

The inoculated plates were incubated at 37 °C and the number of colonies on the Petri plates were counted after 24 h. The colony forming units (CFUs) were calculated by multiplying the number of colonies by the dilution factor. The survival percentage was used to evaluate the antimicrobial effect of particles, which is defined by the following formula:[24]

$$\text{Survival } \% = \frac{\text{Colony number of treated bacteria}}{\text{Colony number of control bacteria}} \times 100. \quad (1)$$

An equal amount of zinc-substituted cobalt ferrite nanopowder obtained from using CA as the chelating agent was coated onto filter papers to perform testing according to the modified Kirby-Bauer method.[25] All samples were placed on the *E. coli* growth LB agar plate and incubated overnight at 37 °C. The zone of inhibition which was the area that bacteria cannot be grown was measured.

RESULTS AND DISCUSSION

Raman analyses

Cobalt ferrite has a cubic inverse spinel structure belonging to the O_h^7 ($Fd3m$) space group. The metallic cations can occupy two types of positions: either surrounded by six oxygen ions forming an octahedron or by four oxygen ions forming a tetrahedron. This structure gives rise to 39 normal modes among which five are Raman active ($A_{1g} + 1E_g + 3T_{2g}$).[26] Figure 1 shows Raman spectra of synthesized cobalt ferrite and zinc-substituted cobalt ferrite ($Co_{(1-x)}Zn_xFe_2O_4$ with $x = 0$, 0.3, 0.5, 0.7, and 1) nanopowders: (a) $CoFe_2O_4$, (b) $Co_{0.7}Zn_{0.3}Fe_2O_4$, (c) $Co_{0.5}Zn_{0.5}Fe_2O_4$, (d) $Co_{0.3}Zn_{0.7}Fe_2O_4$, and (e) $ZnFe_2O_4$. The spectrum of $CoFe_2O_4$ (Fig. 1(a)) consists of broad bands at 311, 470, 571, 619, and a strong band at 693 cm^{-1}. In cobalt ferrite, the octahedral site is occupied by Co and Fe ions and the tetrahedral site is occupied by only the Fe ion. Due to the difference in ionic radii of Co and Fe ions in $CoFe_2O_4$, the Fe–O and Co–O bond distances redistribute between both sites resulting in a doublet-like structure. It has been observed that Raman bands at 690 and 619 cm^{-1} are assigned to $A_{1g}(1)$ and $A_{1g}(2)$ modes reflecting the stretching vibration of Fe^{3+} and O^{2-} ions in octahedral sites (*O-site*), while low frequency bands at 571, 470, and 311 cm^{-1} are assigned to $T_{2g}(3)$, $T_{2g}(2)$, and E_g modes, respectively, which reflect the vibration at the tetrahedral sites (*T-site*).[27]

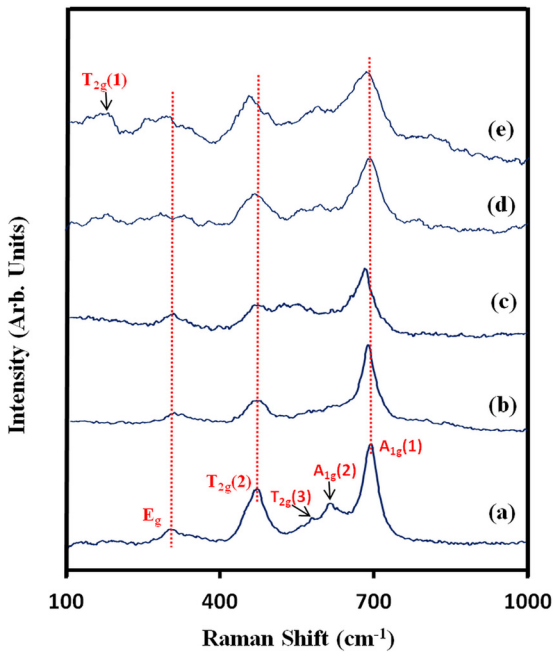

FIG. 1. Raman spectra of the synthesized zinc-substituted cobalt ferrite ($Co_{(1-x)}Zn_xFe_2O_4$ with $x = 0$, 0.3, 0.5, 0.7, and 1) nanopowders: (a) $CoFe_2O_4$, (b) $Co_{0.7}Zn_{0.3}Fe_2O_4$, (c) $Co_{0.5}Zn_{0.5}Fe_2O_4$, (d) $Co_{0.3}Zn_{0.7}Fe_2O_4$, and (e) $ZnFe_2O_4$.

Some changes of the spectra labelled as "b" through to "e" in Fig. 1 are noticed when zinc becomes incorporated into $Co_{(1-x)}Zn_xFe_2O_4$. The $T_{2g}(1)$ mode appears in the Raman band at 207 cm^{-1}, especially with $Co_{0.3}Zn_{0.7}Fe_2O_4$ (d) and $ZnFe_2O_4$ (e) spectra. Moreover, there is some observable decrease in intensity of the 690 cm^{-1} tetrahedral Raman band and all the peaks are shifted towards the lower wave number side. This red shift is attributed to the higher atomic mass of zinc compared to the cobalt ion. In a similar fashion to the spinel ferrite, the distribution of divalent and trivalent cations can change due to migration of metal ions from tetrahedral (A) to octahedral (B) sites and vice versa. These changes could arise from a high degree of cation disorder induced by Zn^{2+} ion incorporation and/or a particle size effect.[28]

FeSEM/EDX analyses

SEM micrographs were analysed to investigate the grain structure of the nanopowders and assist in understanding the development of the grain sizes. Figure 2 shows the SEM images of the synthesized cobalt ferrite and zinc-substituted cobalt ferrite ($Co_{(1-x)}Zn_xFe_2O_4$ with $x = 0$, 0.3, 0.5, 0.7, and 1) nanopowders using CA as a chelating agent: (a) $CoFe_2O_4$, (b) $Co_{0.7}Zn_{0.3}Fe_2O_4$, (c) $Co_{0.5}Zn_{0.5}Fe_2O_4$, (d) $Co_{0.3}Zn_{0.7}Fe_2O_4$, and (e) $ZnFe_2O_4$. The $CoFe_2O_4$ nanopowders, Fig. 2(a), exhibit an angular morphology, showing one or more acute angles formed by adjacent surfaces. Meanwhile, the nanopowders synthesized with Zn doping in Figs. 2(b)–2(e) present particles with irregular shapes and some agglomeration where particles form large clusters. The average of 30 grain sizes measured by IMAGEJ (developed by National Institutes of Health (NIH), USA) for $Co_{(1-x)}Zn_xFe_2O_4$ with $x = 0$, 0.3, 0.5, 0.7, and 1 are 41.12, 42.45, 42.58, 44.79, and 45.65 nm, respectively.

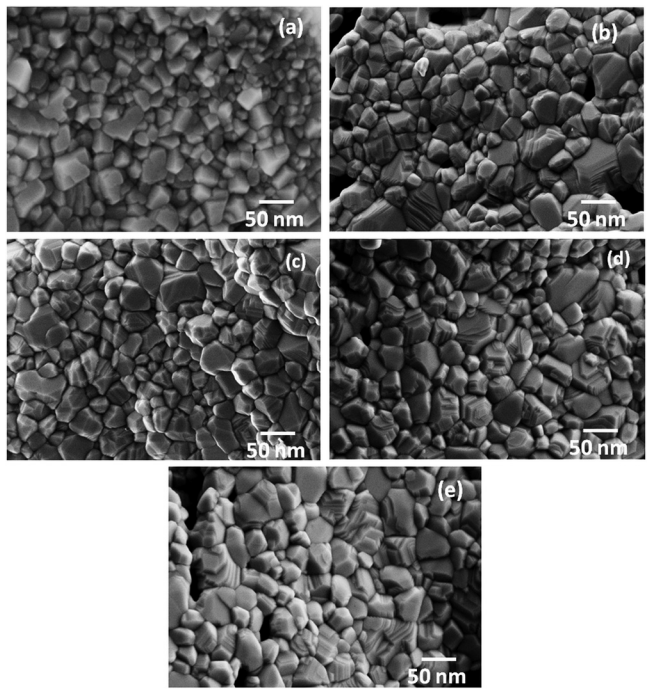

FIG. 2. SEM images of synthesized zinc-substituted cobalt ferrite ($Co_{(1-x)}Zn_xFe_2O_4$ with $x = 0$, 0.3, 0.5, 0.7, and 1) nanopowders: (a) $CoFe_2O_4$, (b) $Co_{0.7}Zn_{0.3}Fe_2O_4$, (c) $Co_{0.5}Zn_{0.5}Fe_2O_4$, (d) $Co_{0.3}Zn_{0.7}Fe_2O_4$, and (e) $ZnFe_2O_4$.

The elemental compositions of synthesized cobalt ferrite and zinc-substituted cobalt ferrite nanopowders ($Co_{(1-x)}Zn_xFe_2O_4$ with $x = 0$, 0.3, 0.5, 0.7, and 1) are listed in Table I. These results indicate that the ratios of Co/Zn/Fe for all of the synthesized nanopowders are almost the same as that of the ideal zinc-substituted cobalt ferrite ($Co_{(1-x)}Zn_xFe_2O_4$) structure, which could confirm that no organic chelating agent remained in the system.

DSC/TGA analyses

DSC/TGA curves of synthesized zinc ferrite and zinc-substituted cobalt ferrite nanopowders: (a) $Co_{0.7}Zn_{0.3}Fe_2O_4$, (b) $Co_{0.5}Zn_{0.5}Fe_2O_4$, (c) $Co_{0.3}Zn_{0.7}Fe_2O_4$, and (d) $ZnFe_2O_4$ obtained from CA as a chelating agent are shown in Fig. 3. Over the temperature range of 25 to 600 °C, the TGA curve exhibits two distinct weight loss steps and the DSC curve presents two exothermic peaks and one endothermic peak. The first weight loss step in the range of 25–150 °C, which was accompanied by an endothermic broad peak around 150 °C in the DSC curve, arises from loss of residual moisture in the powders. The second weight loss step in the range

TABLE I. The elemental composition of synthesized cobalt ferrite and zinc-substituted cobalt ferrite nanopowders.

	at. %			
Ferrites composition	Co	Zn	Fe	O
$CoFe_2O_4$	14.49	…	28.54	56.97
$Co_{0.7}Zn_{0.3}Fe_2O_4$	10.03	4.57	28.51	56.89
$Co_{0.5}Zn_{0.5}Fe_2O_4$	7.36	7.40	28.46	56.78
$Co_{0.3}Zn_{0.7}Fe_2O_4$	4.28	10.04	28.67	57.01
$ZnFe_2O_4$	…	14.31	28.75	56.94

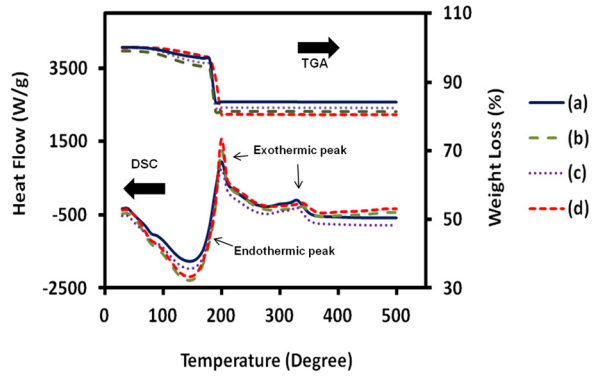

FIG. 3. DSC/TGA curves of synthesized zinc-substituted cobalt ferrite nanopowders: (a) $Co_{0.7}Zn_{0.3}Fe_2O_4$, (b) $Co_{0.5}Zn_{0.5}Fe_2O_4$, (c) $Co_{0.3}Zn_{0.7}Fe_2O_4$, and (d) $ZnFe_2O_4$.

of 170–200 °C and the sharp exothermic peak around 200 °C is associated with the combustion of nitrates and the remaining organic substances. Moreover, the small exothermic peak at nearly 350 °C refers to the oxidation of carbon from the CA by oxygen in the air that forms carbon dioxide and releases heat. No weight loss was observed above 350 °C, implying the presence of only cobalt ferrite and zinc-substituted cobalt ferrite within this temperature range.

XRD analysis

X-ray diffraction patterns of synthesized cobalt ferrite and zinc-substituted cobalt ferrite nanopowders: (a) $Co_{0.7}Zn_{0.3}Fe_2O_4$, (b) $Co_{0.5}Zn_{0.5}Fe_2O_4$, (c) $Co_{0.3}Zn_{0.7}Fe_2O_4$, and (d) $ZnFe_2O_4$, obtained from sol-gel methods using CA as the chelating agent and calcined at 800 °C for 4 h are shown in Fig. 4.

The peaks at 30.08°, 35.44°, 37.06°, 43.06°, 53.45°, 56.98°, and 62.59° are indexed as the reflection planes of (220), (311), (222), (400), (422), (511), and (440), respectively. Analysis of the XRD patterns of all samples confirmed the formation of the cubic spinel structure as the main characteristic peak. Moreover, no XRD peaks corresponding to the other phases, such as α-Fe_2O_3, CoO, ZnO, Co_2O_3 or Co_3O_4 were noticed. The results are in good agreement with Zi *et al.*'s.[29] Thus, this experimental observation concludes that zinc was completely substituted into the cobalt ferrite lattice synthesized by calcination of the precursor and chelating agent derived from the sol-gel process.

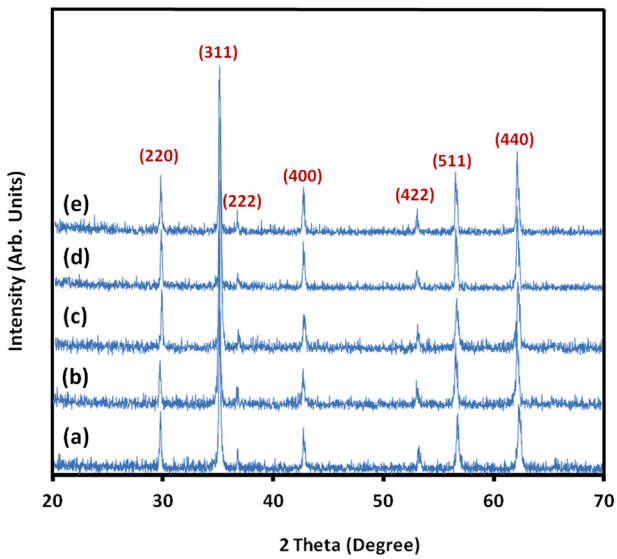

FIG. 4. X-ray diffraction patterns of synthesized zinc-substituted cobalt ferrite ($Co_{(1-x)}Zn_xFe_2O_4$ with $x = 0$, 0.3, 0.5, 0.7, and 1) nanopowders: (a) $CoFe_2O_4$, (b) $Co_{0.7}Zn_{0.3}Fe_2O_4$, (c) $Co_{0.5}Zn_{0.5}Fe_2O_4$, (d) $Co_{0.3}Zn_{0.7}Fe_2O_4$, and (e) $ZnFe_2O_4$.

The crystallite size D was calculated according to the Scherer equation[30]

$$D = \frac{0.9\lambda}{\beta \cos\theta}, \tag{2}$$

where λ is the wavelength of the radiation, θ is the diffraction angle, and β is the full width at half maximum (FWHM) measurement of the diffraction peak. The lattice parameter was calculated according to the formula

$$a = d_{hkl}\sqrt{(h^2 + k^2 + l^2)}. \tag{3}$$

The reflection plane (311) was used to calculate both the crystallite size and lattice constant since this has the maximum diffraction intensity. The crystallite size and lattice constant of the cobalt ferrite and zinc-substituted cobalt ferrite nanopowders ($Co_{(1-x)}Zn_xFe_2O_4$ with $x = 0$, 0.3, 0.5, 0.7, and 1) synthesized using citric acid as chelating agent have been summarized in Table II.

The calculated lattice constant a (using the d value and respective hkl (311) parameters) increased from 8.385 Å to 8.415 Å for the samples calcined at 800 °C with increasing zinc substitution from 0 to 1. The relationship between zinc substitution and lattice parameter is near linear as shown in Fig. 5. According to Vegard's law,[31] the linear relationship implies the formation of homogeneous $Co_{(1-x)}Zn_xFe_2O_4$ solid solutions. The increase in the lattice parameter results from the difference in the Zn^{2+} (0.74 Å) and Co^{2+} (0.72 Å) ionic radii.[32] Moreover, the crystallite size of cobalt ferrite and zinc-substituted cobalt ferrite nanopowders determined by taking the FWHM of the (311) peak was found to lie in the range of 40–50 nm; values that agree well with those measured from IMAGEJ.

Contact angle and surface roughness measurement

The hydrophilicity and surface roughness are presented in Table III. The surfaces of cobalt ferrite and zinc-substituted cobalt ferrite nanopowders are hydrophilic since the water contact angles are less than 90°. The results indicate that no significant differences in surface wettability could be detected

TABLE II. The crystallite size and lattice constant of the cobalt ferrite and zinc-substituted cobalt ferrite nanopowders.

Ferrites composition	Lattice parameter (Å)	Crystallite size (nm)
$CoFe_2O_4$	8.385	43
$Co_{0.7}Zn_{0.3}Fe_2O_4$	8.391	43
$Co_{0.5}Zn_{0.5}Fe_2O_4$	8.401	44
$Co_{0.3}Zn_{0.7}Fe_2O_4$	8.409	45
$ZnFe_2O_4$	8.415	45

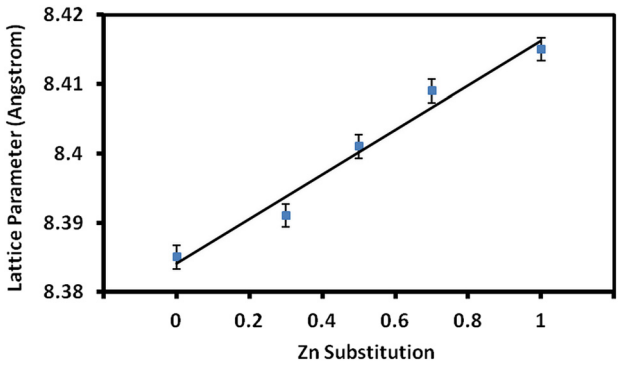

FIG. 5. Dependence of the lattice parameter, determined from XRD peak positions, upon the extent of zinc doping.

between cobalt ferrite nanopowders and zinc-substituted cobalt ferrite nanopowders. In terms of the surface roughness of nanopowders, pure cobalt ferrite presents the smoothest surface followed by $Co_{0.7}Zn_{0.3}Fe_2O_4$, $Co_{0.5}Zn_{0.5}Fe_2O_4$, $Co_{0.3}Zn_{0.7}Fe_2O_4$, and $ZnFe_2O_4$, respectively. These results are in good agreement with the previous XRD results in Table II, which revealed that pure cobalt ferrite exhibited the smallest crystallite size.

Antibacterial activities of the samples

The contact biocidal property of all ferrite nanopowders obtained from CA was investigated using a modified Kirby-Bauer technique.[25] Filter papers were partially covered with and without ferrite nanopowders and placed on a lawn of *E. coli* in an agar plate. The contact antibacterial property can be measured by the clear zone of inhibition around the filter papers after an incubation of one day, Fig. 6. The diameter of the inhibition zone for the zinc-substituted cobalt ferrite is larger than that of pure cobalt ferrite nanopowders, especially when the zinc concentration was increased. The result indicates that the zinc-substituted cobalt ferrite nanopowders have a more effective contact biocidal property than pure cobalt ferrite nanopowders.

The antibacterial activities of the zinc-substituted cobalt ferrite nanopowders against *E. coli* and *S. aureus* are shown in Fig. 7. All tests were repeated ten times for statistical studies after culture incubation at 37 °C overnight. The concentration of cobalt ferrite nanopowders was fixed at 1 g/l. Compared to the control, zinc-substituted cobalt ferrite nanopowders inhibit the growth of both *E. coli* and *S. aureus*, and the *E. coli* killing rate of zinc-substituted cobalt ferrite nanopowders is higher than those *S. aureus* killing rate. Their antibacterial abilities become stronger with increasing zinc substitution concentration.

TABLE III. Surface wettability and roughness for synthesized cobalt ferrite and zinc-substituted cobalt ferrite nanopowders.

Samples	Water contact angle (deg)	Surface roughness, Ra (μm)
$CoFe_2O_4$	62 ± 0.2	3.54 ± 0.3
$Co_{0.7}Zn_{0.3}Fe_2O_4$	63 ± 0.1	3.98 ± 0.2
$Co_{0.5}Zn_{0.5}Fe_2O_4$	64 ± 0.3	4.35 ± 0.3
$Co_{0.3}Zn_{0.7}Fe_2O_4$	65 ± 0.2	4.57 ± 0.1
$ZnFe_2O_4$	66 ± 0.2	4.97 ± 0.3

A substantial amount of research has been conducted to investigate the effect of substratum surface chemistry on bacterial adhesion, and the recent trend has focused on the role that surface wettability and roughness play in the bacterial attachment process.[33,34] It has been claimed that both surface wettability and roughness have significant influence on bacterial attachment on the substratum.[35] However, the surface wettability and roughness, in this investigation, may not play a role with respect to the antibacterial activity of nanopowders since no significant differences in surface wettability and roughness could be detected between cobalt ferrite nanopowders and zinc-substituted cobalt ferrite nanopowders.

There are several possible mechanisms for the antibacterial action of zinc ceramic nanopowders. One suggestion is that zinc binds to the membranes of microorganisms, in a fashion similar to mammalian cell attachment; thereby prolonging the lag phase of the growth cycle and increasing the generation time of the organisms so that it takes more time for each organism to complete cell division.[36] Another proposition maintained that the main chemical species contributing to the occurrence of the antibacterial activity were assumed to be active oxides, i.e., hydrogen peroxide (H_2O_2) and super-oxide (O_2^-), generated from the surface of these zinc ceramics.[37] These active oxides readily penetrate the cell wall of bacteria and cause cell destruction.[38]

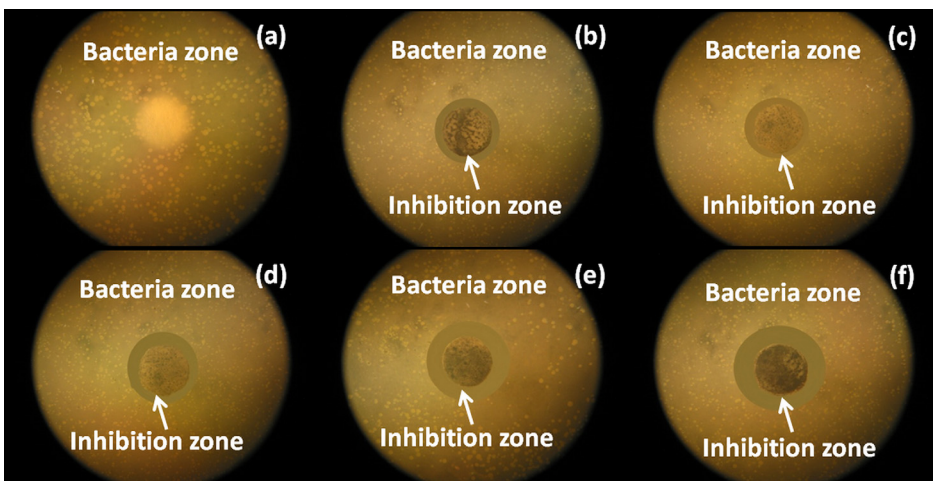

FIG. 6. Image of *E. coli* incubated for 24 h at 37 °C together with filter paper: (a) without cobalt ferrite nanopowders, (b) $CoFe_2O_4$, (c) $Co_{0.7}Zn_{0.3}Fe_2O_4$, (d) $Co_{0.5}Zn_{0.5}Fe_2O_4$, (e) $Co_{0.3}Zn_{0.7}Fe_2O_4$, and (f) $ZnFe_2O_4$.

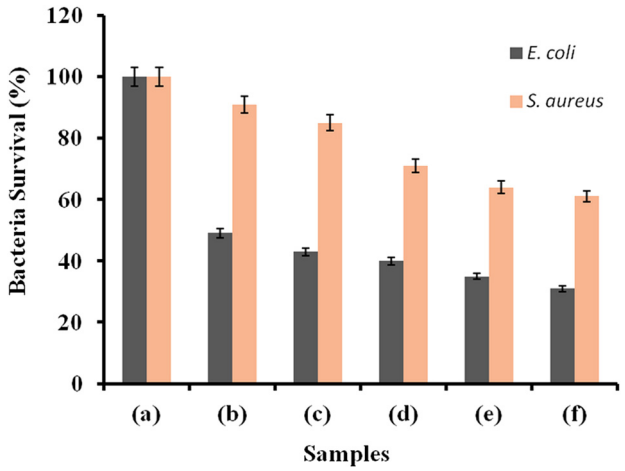

FIG. 7. Antibacterial testing against *E. coli* and *S. aureus* of synthesized zinc-substituted cobalt ferrite ($Co_{(1-x)}Zn_xFe_2O_4$ with $x = 0$, 0.3, 0.5, 0.7, and 1) nanopowders: (a) without cobalt ferrite nanopowders, (b) $CoFe_2O_4$, (c) $Co_{0.7}Zn_{0.3}Fe_2O_4$, (d) $Co_{0.5}Zn_{0.5}Fe_2O_4$, (e) $Co_{0.3}Zn_{0.7}Fe_2O_4$, and (f) $ZnFe_2O_4$.

The penetration rate of active oxides through the bacteria cell wall plays an important role in the killing rate of zinc ceramic nanopowders against bacteria. Furthermore, it is known that the structure and the chemical composition of the cell wall are quite different between *E. coli* and *S. aureus*, that is, *E. coli* has a cell wall consisting of lipid A, lipopolysaccharide and peptidoglycan, whereas the cell wall of *S. aureus* consists mainly of peptidoglycan. These results indicate that active oxides generated from zinc-substituted cobalt ferrite have more capability to penetrate the cell wall and decrease the cell division of *E. coli* rather than *S. aureus*. However, the factual interaction mechanism between bacteria (*E. coli* and *S. aureus)* and zinc-substituted cobalt ferrite nanopowders needs to be investigated further.

CONCLUSIONS

A sol-gel technique for synthesizing zinc-substituted cobalt ferrite nanopowders that employs citric acid as a chelating agent was developed. Zinc-substituted cobalt ferrite nanopowders formed a cubic spinel structure and exhibited irregular morphology with a crystallite size in the range of 40–50 nm. Increasing the concentration of zinc substitution has no significant effect on the water contact angle and surface roughness. The substitution of zinc in cobalt ferrite nanopowders improved significantly the antibacterial activity against *E. coli* and *S. aureus*. The antibacterial activity of zinc-substituted cobalt ferrite nanopowders against *E. coli* was higher than *S. aureus*. In the test of LB-agar plates, the zinc-substituted cobalt ferrite nanopowders exhibited surface-dependent antibacterial activities. There is potential that zinc-substituted cobalt ferrite nanopowders could be used in drug delivery systems as well as in other biomedical and biotechnology applications.

ACKNOWLEDGMENTS

Mr. N. Sanpo is the recipient of Swinburne University Postgraduate Research Award (SUPRA).

[1]X. Meng, H. Li, J. Chen, L. Mei, K. Wang, and X. Li, J. Magn. Magn. Mater. **321**(9), 1155–1158 (2009).
[2]L. X. Phua, F. Xu, Y. G. Ma, and C. K. Ong, Thin Solid Films **517**(20), 5858–5861 (2009).
[3]M. Sugimoto, J. Am. Ceram. Soc. **82**(2), 269–280 (1999).
[4]M. P. Pileni, Adv. Funct. Mater. **11**(5), 323–336 (2001).
[5]C. Liu, B. Zou, A. J. Rondinone, and Z. J. Zhang, J. Phys. Chem. B **104**(6), 1141–1145 (2000).
[6]L. Zhen, K. He, C. Y. Xu, and W. Z. Shao, J. Magn. Magn. Mater. **320**(21), 2672–2675 (2008).
[7]E. Katz, A. N. Shipway, and I. Willner, in *Nanoparticles* (Wiley-VCH Verlag GmbH & Co. KGaA, 2005), pp. 368–421.
[8]D.-H. Kim, D. E. Nikles, D. T. Johnson, and C. S. Brazel, J. Magn. Magn. Mater. **320**(19), 2390–2396 (2008).
[9]D. Jamon, F. Donatini, A. Siblini, F. Royer, R. Perzynski, V. Cabuil, and S. Neveu, J. Magn. Magn. Mater. **321**(9), 1148–1154 (2009).
[10]G. Vaidyanathan and S. Sendhilnathan, Physica B **403**(13–16), 2157–2167 (2008).
[11]K. Byrappa, S. Ohara, and T. Adschiri, Adv. Drug Delivery Rev. **60**(3), 299–327 (2008).
[12]A. S. Buteică, D. E. Mihaiescu, A. M. Grumezescu, B. Ş. Vasile, A. Popescu, O. M. Mihaiescu, and R. Cristescu, Dig. J. Nanomater. Bios. **5**(4), 927–932 (2010).
[13]S. Sun, H. Zeng, D. B. Robinson, S. Raoux, P. M. Rice, S. X. Wang, and G. Li, J. Am. Chem. Soc. **126**(1), 273–279 (2004).
[14]M. H. Yousefi, S. Manouchehri, A. Arab, M. Mozaffari, G. R. Amiri, and J. Amighian, Mater. Res. Bull. **45**(12), 1792–1795 (2010).
[15]M. U. Islam, F. Aen, S. B. Niazi, M. Azhar Khan, M. Ishaque, T. Abbas, and M. U. Rana, Mater. Chem. Phys. **109**(2–3), 482–487 (2008).
[16]C.-K. Kim, J.-H. Lee, S. Katoh, R. Murakami, and M. Yoshimura, Mater. Res. Bull. **36**(12), 2241–2250 (2001).
[17]I. H. Gul and A. Maqsood, J. Alloys Compd. **465**(1–2), 227–231 (2008).
[18]G. De, G. Mattei, P. Mazzoldi, C. Sada, G. Battaglin, and A. Quaranta, Chem. Mater. **12**(8), 2157–2160 (2000).
[19]M. Grigorova, H. J. Blythe, V. Blaskov, V. Rusanov, V. Petkov, V. Masheva, D. Nihtianova, L. M. Martinez, J. S. Muñoz, and M. Mikhov, J. Magn. Magn. Mater. **183**(1–2), 163–172 (1998).
[20]A. M. R. d. F. Teixeira, T. Ogasawara, and M. C. d. S. Nóbrega, Mater. Res. **9**, 257–262 (2006).
[21]P. Yaseneva, M. Bowker, and G. Hutchings, Phys. Chem. Chem. Phys. **13**(41), 18609–18614 (2011).
[22]P. Pandya, H. Joshi, and R. Kulkarni, J. Mater. Sci. **26**(20), 5509–5512 (1991).
[23]O. M. Hemeda, Phase Transitions **51**(1-2), 87–95 (1994).
[24]Z. Lu, C. M. Li, H. Bao, Y. Qiao, Y. Toh, and X. Yang, Langmuir **24**(10), 5445–5452 (2008).
[25]T. D. Wikins, L. V. Holdeman, I. J. Abramson, and W. E. Moore, Antimicrob. Agents Chemother. **1**(6), 451–459 (1972).
[26]T. Yu, Z. X. Shen, Y. Shi, and J. Ding, J. Phys. Condens. Matter **14**(37), L613–L618 (2002).
[27]D. Varshney, K. Verma, and A. Kumar, J. Mol. Struct. **1006**(1-3), 447–452 (2011).
[28]S. Ayyappan, G. Panneerselvam, M. P. Antony, N. V. Rama Rao, N. Thirumurugan, A. Bharathi, and J. Philip, J. Appl. Phys. **109**(8), 084303 (2011).
[29]Z. Zi, Y. Sun, X. Zhu, Z. Yang, J. Dai, and W. Song, J. Magn. Magn. Mater. **321**(9), 1251–1255 (2009).
[30]J. Robertson, Acta Crystallogr. Sect. A **35**(2), 350 (1979).
[31]I. P. Parkin, Appl. Organomet. Chem. **14**(4), 227–228 (2000).
[32]Y. Köseoğlu, A. Baykal, M. S. Toprak, F. Gözüak, A. C. Başaran, and B. Aktaş, J. Alloys Compd. **462**(1–2), 209–213 (2008).
[33]R. Bos, H. C. Van Der Mei, and H. J. Busscher, FEMS Microbiol. Rev. **23**(2), 179–229 (1999).
[34]M. G. Katsikogianni and Y. F. Missirlis, J. Mater. Sci.: Mater. Med. **21**(3), 963–968 (2010).
[35]A. V. Singh, V. Vyas, R. Patil, V. Sharma, P. E. Scopelliti, G. Bongiorno, A. Podestà, C. Lenardi, W. N. Gade, and P. Milani, PLoS ONE **6**(9), e25029 (2011).
[36]L. L. Radke, B. L. Hahn, D. K. Wagner, and P. G. Sohnle, Clin. Immunol. Immunopathol. **73**(3), 344–349 (1994).
[37]O. Yamamoto and J. Sawai, Bull. Chem. Soc. Jpn. **74**(9), 1761–1765 (2001).
[38]J. Sawai, S. Shoji, H. Igarashi, A. Hashimoto, T. Kokugan, M. Shimizu, and H. Kojima, J. Ferment. Bioeng. **86**(5), 521–522 (1998).